A

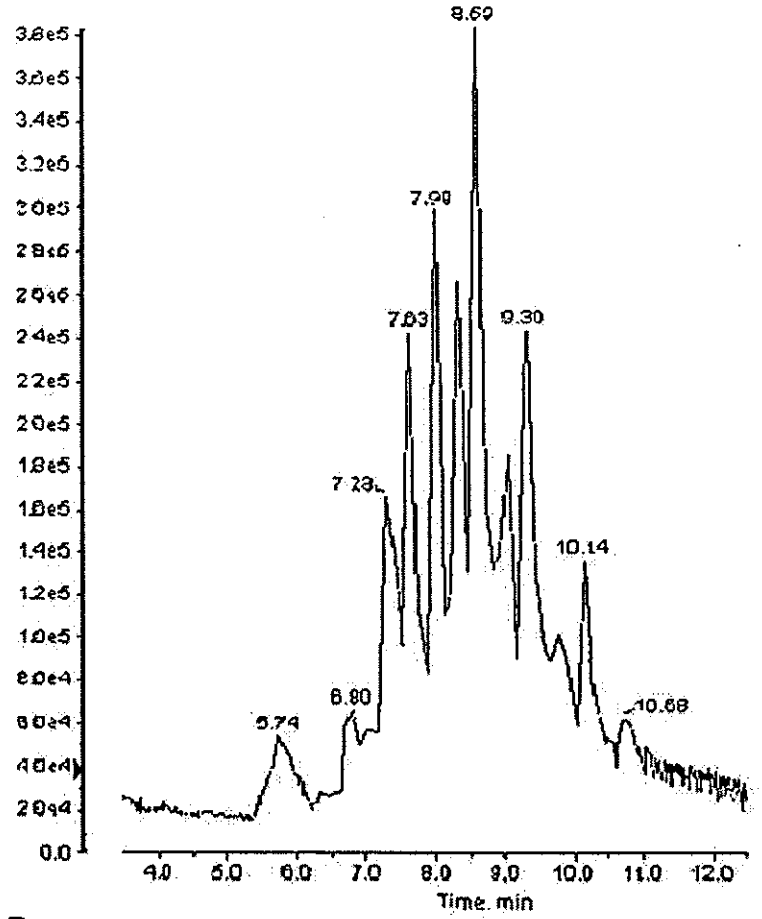

B

R.Time	ion observed	Mr(expt)	Mr(calc)	Delta	Miss	Peptide
5.39	470.27	938.53	938.47	0.06	0	AETYTGGLK
5.56	586.27	1170.52	1170.50	0.03	0	SVDGDQTYMR
5.90	568.77	1135.53	1135.49	0.04	0	NMSTYVDYK + Oxidation (M)
6.80	443.72	885.42	884.41	1.00	0	GNGFATYR
7.26	607.65	1819.91	1819.84	0.07	1	RTDDQNSPLYIGNGDR
7.28	560.76	1119.51	1119.49	0.02	0	NMSTYVDYK
7.63	432.55	1294.62	1294.58	0.04	0	VDGLHYFSDDK
7.99	645.79	1289.56	1289.57	-0.00	0	FQDVGSFDYGR
8.11	862.76	2585.27	2584.20	1.06	1	TDDQNSPLYIGNGDRAETYTGGLK
8.35	720.33	1438.66	1438.68	-0.02	0	YVDVGATYYFNK
8.59	785.38	2353.12	2353.10	0.02	0	YDANNIYLAAQYTQTYNATR
10.14	1117.07	2232.12	2232.09	0.04	0	NTDFFGLVDGLNFAVQYQGK

C

1 MKVKVLSLLV PALLVAGAAN AAEVYNKDGN KLDLYGKVDG LHYFSDDKSV

51 DGDQTYMRLG FKGETQVTDQ LTGYGQWEYQ IQGNSAENEN NSWTRVAFAG

101 LKFQDVGSFD YGRNYGVVYD VTSWTDVLPE FGGETYGSDN FMQQRGNGFA

151 TYRNTDFFGL VDGLNFAVQY QGKNGSVSGS GNTYNGREAL RQNGDGVGGS

201 ITYDYEGFGI GAAVSSGFRT DDQNSPLYIG NGDRAETYTG GLKYDANNIY

251 LAAQYTQTYN ATRVGSLGVA NKAQNFEAVA QYQEDFGLRP SLAYIQSKGK

301 NLGVINGRNY DDEDILKYVD VGATYYFNKN MSTYVDYKIN LLDTNQFTRD

FIG. 2. **LC/MS analysis of the PK-resistant protein in the urine.** Peptides from tryptic digestion of the PK-resistant protein in the urine of sCJD-3 were separated using MAGIC 2002 liquid chromatography and the elute were analyzed by MS. *A*, base peak mass chromatogram of the 37-kDa protein, each peak is labeled with the retention time. *B*, molecular mass and amino acid sequence of each peak originating from the 37-kDa protein. All the determined amino acid sequences were identical to that of OMP of *E. coli* (OmpC precursor) based on the results of the data base search. *R. Time*, retention time; *Mr(expt)*, molecular weight in the experiment; *Mr(calc)*, molecular weight in calculation. *C*, amino acid sequence of OmpC of *E. coli* was shown. *Bold style letters* indicate sequences covered by the results of the LC/MS analysis. The sequence identified by N-terminal sequencing analysis is shown with an *underline*.

TABLE III

Results of the N-terminal sequence of PK-resistant signal in patients' urine

Amino acid sequences were queried against entries for all species in the SwissProt database using the FASTA search programs offered by GenomeNet. PK-resistant protein bands with molecular mass about 37 kDa were subjected to the analysis.

Patient ID	N-terminal sequence	Protein identification and species
Sporadic CJD		
sCJD-1[a]	AEIYNKDGNK	OmpC, *K. pneumoniae*
sCJD-2[a]	AEVYNKDGNK	OmpC, *E. coli*
sCJD-3[a]	AEVYNKDGNK	OmpC, *E. coli*
sCJD-4	AEVYNKJDGNKLDLYGKVDGL	OmpC, *E. coli*
sCJD-5	AEIYNKDGNKLDLYG	OmpC, *K. pneumoniae*, or OmpF, *S. typhimurium*
sCJD-6[a]	AEVYNKDGNKLDLYG	OmpC, *E. coli*
sCJD-7	AEVLNKDONK	OmpC, *E. coli*
sCJD-8[a]	AEVYNKDGNKL	OmpC, *E. coli*
sCJD-9[a]	AEVYDKDGKNLDL	Omp *Sodalis glossinidius*
sCJD-10[a]	AEVYNKDGNKL	OmpC, *E. coli*
sCJD-11[a]	AEVYNKDGNKLDLYG	OmpC, *E. coli*
Dural graft-associated CJD		
1	AEVYNKDGNKLDLYG	OmpC, *E. coli*
2[a]	AEIYNKDGNKLDLYG	OmpC *K. pneumoniae*, or OmpF, *S. typhimurium*

[a] Urine samples were re-suspended in STE buffer containing 2% Sarkosyl as described by Shaked *et al.* (7) or otherwise in PBS containing 0.5% Nonidet P-40 and 0.5% deoxyehdate.

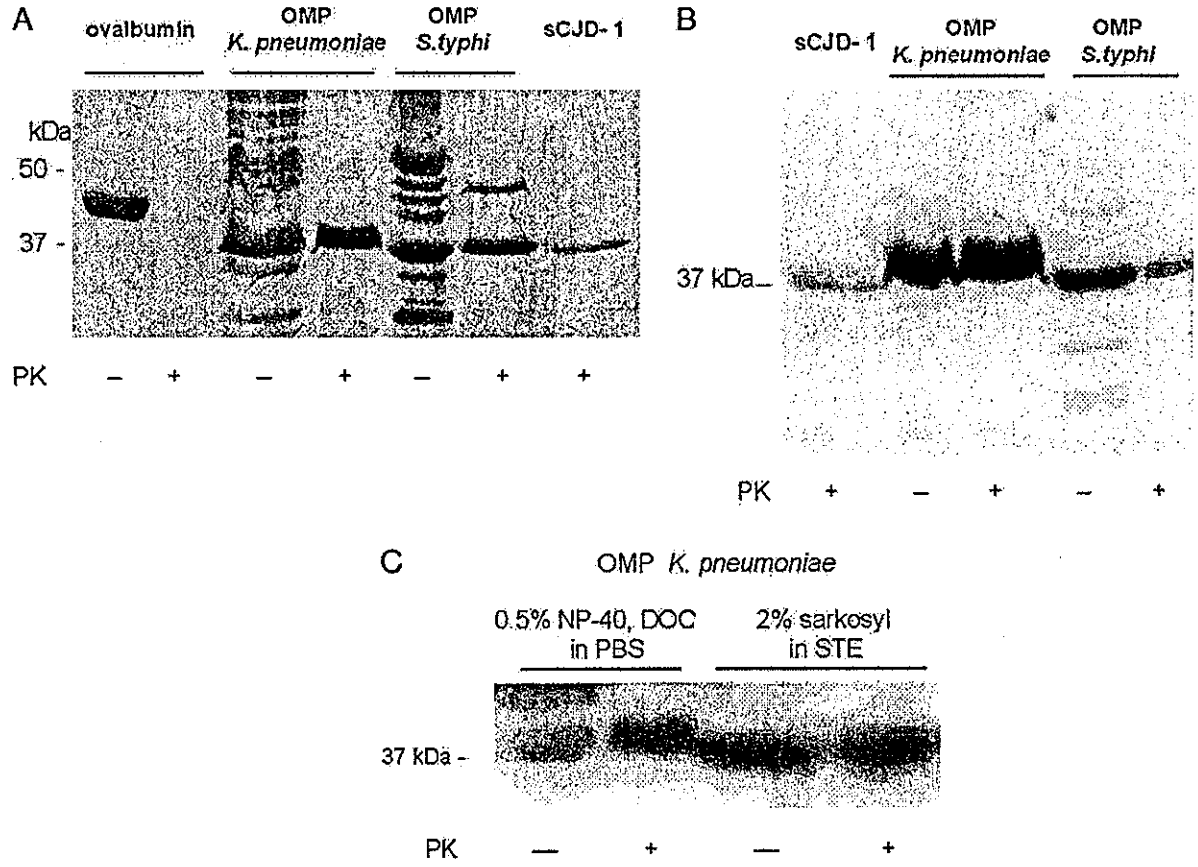

FIG. 3. **PK sensitivity and immunoreactivity of OMPs of *K. pneumoniae* and *S. typhimurium*.** *A*, OMPs isolated from *K. pneumoniae* and *S. typhimurium*, and protein isolated from 15 ml of urine of sCJD-1 patient were digested with PK. Proteins were re-suspended in PBS (pH 7.4) containing 0.5% Nonidet P-40 and 0.5% deoxycholate (*DOC*). An OMP homogenate containing 30 μg of protein was applied in each lane. Fifteen micrograms of ovalbumin was used as a control. After the electrophoretic separation, the polyacrylamide gel was stained with Coomassie Brilliant Blue. *B*, after separation by SDS-PAGE, the gel was blotted onto a polyvinylidene difluoride membrane. Rabbit-derived $F(ab')_2$ fragment of anti-mouse IgG was used as a probe. *C*, OMPs isolated from *K. pneumoniae* were re-suspended in PBS (pH 7.4) containing 0.5% Nonidet P-40 and 0.5% deoxycholate or in STE buffer containing 2% Sarkosyl and digested with PK. The blot was incubated with the rabbit-derived $F(ab')_2$ fragment of anti-mouse IgG.

OMPs are heat modifiable and resistant to trypsin (12). In this study, we have confirmed that OMPs of *K. pneumoniae* and *S. typhimurium* were also resistant to PK and the resulting molecules migrated around 37 kDa on SDS-PAGE.

OMPs act as a determinant of the permeability of antimicrobial agents and affect the interaction between bacteria and host defense mechanisms (13). Whereas it is known that the OMPs of *K. pneumoniae* bind to C1q (14), there are no previous reports that indicate the binding between OMPs and IgG. We found that OMPs bound non-specifically to IgG (several kinds of antibodies) during the procedure of Western blot analysis. Because protein A, a cell wall component of *S. aureus*, has been known to bind to the Fc region of IgG (15), we hypothesized that OMPs might also bind to IgG in the same manner. Contrary to our expectations, OMPs still reacted with the $F(ab')_2$ fragment of anti-mouse IgG, indicating that they bound to IgG

in a manner that is different from that of protein A with immunoglobulins. It might be suggested that accidentally acquired antibodies against bacterial OMPs in the serum of immunized animals might react with OMPs, resulting in protease-resistant signals. However, Western blot analysis using anti-mouse IgG produced by a phage-display method, for example, would be required to exclude this hypothesis.

Our findings were not consistent with those of a previous report by Shaked *et al.* (7). They showed that PK-resistant proteins in the urine of patients and animals affected with prion diseases were prion protein and termed them $UPrP^{Sc}$. The signal of $UPrP^{Sc}$ showed a downward shift after PK digestion resulting in a 32-kDa fragment, whereas the majority of PK-resistant signals that we detected did not show a significant downward shift. Apart from the 37-kDa PK-resistant signal, a faint 22-kDa signal was observed in some patients and a 28-kDa signal was observed in both patients and controls. N-terminal sequencing revealed that these signals were fragments of OMPs and PK molecules, respectively. In this study, we did not observe any PK-resistant signals migrating around 32 kDa, which was detected by Shaked *et al.* (7) in the urine of patients. Therefore, the possibility that the PK-resistant molecule in this study might be a different molecule from $UPrP^{Sc}$, as demonstrated by Shaked *et al.* (7), was not excluded.

However, the high incidence of OMPs (37-kDa PK-resistant signals, non-specifically bind to immunoglobulins) in the urine of patients affected with prion diseases, irrespective of the assay conditions, indicated that bacterial contamination would always have to be considered in the application of a "$UPrP^{Sc}$ assay" in the diagnosis of human prion diseases. Our findings suggest that PrP^{Sc} and PrP^{C} may not always exist or could exist at a very low level in urine, and bacterial contamination may often cause false detection of a PK-resistant isoform of prion protein in urine and a misinterpretation of results.

We have also analyzed the urine protein of mice experimentally infected with a prion agent. The PK-resistant signals of 25 kDa were found in the urine of affected mice, but these signals were also detectable using a secondary antibody alone, omitting the labeling by a primary antibody (data not shown). Furthermore, N-terminal sequencing analysis revealed that these PK-resistant signals in mice urine were OMPs of *Pseudomonas aeruginosa*.

In conclusion, the detection of $UPrP^{Sc}$ is not useful or reliable for ante-mortem, definite diagnosis of human prion diseases in the present situation. Further improvement in sensitivity and specificity of this assay may make it a powerful diagnostic tool for prion diseases in the future.

Acknowledgments—We thank Dr. Mitsuhiro Tsujihata, Nagasaki North Hospital, Nagasaki, Japan, and Dr. Shunsuke Matsumoto, Second Kawanami Hospital, Fukuoka, Japan, for providing urine samples of the control groups used in this study. We also thank Dr. Mitsuo Takahashi and Dr. Tatsuo Yamada, Department of the Fifth Internal Medicine, Fukuoka University, Japan, for critically reading the manuscript.

REFERENCES

1. World Health Organization (2000) *WHO Infection Control Guidelines for Transmissible Spongiform Encephalopathies: Report of a WHO Consultation, Geneva, Switzerland, 23–26 March 1999*, Section 2.2, Communicable Disease Surveillance and Response (CSR), WHO
2. Demaerel, P., Baert, A. L., Vanopdenbosch, L., Robberecht, W., and Dom, R. (1997) *Lancet* **349**, 847–848
3. Hsich, G., Kenny, K., Gibbs, C. J., Lee, K. H., and Harrington, M. G. (1996) *N. Eng. J. Med.* **335**, 924–930
4. Riemenschneider, M., Wagenpfeil, S., Vanderstichele, H., Otto, M., Wiltfang, J., Kretzschmar, H., Vanmechelen, E., Forstl, H., and Kurz, A. (2003) *Mol. Psychiatry* **8**, 343–347
5. Castellani, R., Parchi, P., Stahl, J., Capellari, S., Cohen, M., and Gambetti, P. (1996) *Neurology* **46**, 1690–1693
6. Bieschke, J., Giese, A., Schulz-Schaeffer, W., Zerr, I., Poser, S., Eigen, M., and Kretzschmar, H. (2000) *Proc. Natl. Acad. Sci. U. S. A.* **97**, 5468–5473
7. Shaked, G. M., Shaked, Y., Kariv-Inbal, Z., Halimi, M., Avraham, I., and Gabizon, R. (2001) *J. Biol. Chem.* **276**, 31479–31482
8. Wilm, M., Shevchenko, A., Houthaeve, T., Breit, S., Schweigerer, L., Fotsis, T., and Mann, M. (1996) *Nature* **379**, 466–469
9. Morgenstern, J. P., Griffith, I. J., Brauer, A. W., Rogers, B. L., Bond, J. F., Chapman, M. D., and Kuo, M. C. (1991) *Proc. Natl. Acad. Sci. U. S. A.* **88**, 9690–9694
10. Hernández-Allés, S., Albertí, S., Álvarez, D., Doménech-Sánchez, A., Martínez-Martínez, L., Gil, J., Tomás, J. M., and Benedí, V. J. (1999) *Microbiology* **145**, 673–679
11. Weiss, M. S., Abele, U., Weckesser, J., Welte, W., Schiltz, E., and Schulz, G. E. (1991) *Science* **254**, 1627–1630
12. Albertí, S., Rodríquez-Quiòones, F., Schirmer, T., Rummiel, G., Tomás, J. M., Rosenbusch, J. P., and Benedí, V. J. (1995) *Infect. Immun.* **63**, 903–910
13. Benz, R. (1994) in *Bacterial Cell Walls* (Ghuysen, J.-M., and Hackenbeck, R., eds) pp. 397–424, Elsevier, Amsterdam
14. Albertí, S., Marqués, G., Camprubí, S., Merino, S., Tomás, J. M., Vivanco, F., and Benedí, V. J. (1993) *Infect. Immun.* **61**, 852–860
15. Kessler, S. W. (1975) *J. Immunol.* **115**, 1617–1624

Available online at www.sciencedirect.com
SCIENCE DIRECT®
Biochemical and Biophysical Research Communications 319 (2004) 1247–1252
BBRC
www.elsevier.com/locate/ybbrc

Doppel-induced Purkinje cell death is stoichiometrically abrogated by prion protein

Naohiro Yamaguchi,[a] Suehiro Sakaguchi,[a,b,*] Kazuto Shigematsu,[c] Nobuhiko Okimura,[a] and Shigeru Katamine[a]

[a] *Department of Molecular Microbiology and Immunology, Nagasaki University Graduate School of Biomedical Sciences, Nagasaki 852-8523, Japan*
[b] *PRESTO, Japan Science and Technology Agency, 4-1-8 Honcho Kawaguchi, Saitama, Japan*
[c] *Department of Pathology, Nagasaki University Graduate School of Biomedical Sciences, Nagasaki 852-8523, Japan*

Received 17 May 2004
Available online 4 June 2004

Abstract

Mice devoid of prion protein (PrP) exhibiting ataxia and Purkinje cell degeneration, such as Ngsk *Prnp*$^{-/-}$ mice, ectopically express PrP-like protein, Dpl, in neurons including Purkinje cells. In this study, two types of transgenic (tg) mice expressing Dpl in neurons, tg(N-Dpl), or Purkinje cells only, tg(P-Dpl), were generated on the background of non-ataxic Zrch I *Prnp*$^{-/-}$ mice. In contrast to the tg mice with the *Prnp*$^{+/+}$ background, both tg mice with the *Prnp*$^{-/-}$ alleles developed Purkinje cell degeneration after incubation periods inversely correlated to the levels of Dpl. Some tg mice hemizygous for *Prnp* allele also developed disease but much later than those carrying the *Prnp*$^{-/-}$ alleles. This indicates that Dpl expressed by Purkinje cells itself is toxic to the cells, and that the neurotoxicity is stoichiometrically antagonized by PrP.
© 2004 Elsevier Inc. All rights reserved.

Keywords: Prion protein; Doppel; Neurodegeneration; Purkinje cell; Knockout mice

The normal prion protein (PrP^C) is a glycosylphosphatidylinositol (GPI)-anchored protein expressed abundantly in the central nervous system, in particular by neurons [1,2]. Five independent lines of mice devoid of PrP^C, designated *Prnp*$^{-/-}$ mice, have been so far generated using different targeting strategies. The first two lines of *Prnp*$^{-/-}$ mice, Zrch I and Npu, developed and grew normally [3,4]. In contrast, other lines of mice, Ngsk, Rcm0, and Zrch II, exhibited ataxia and Purkinje cell degeneration [5–7]. We confirmed that the phenotypes in Ngsk *Prnp*$^{-/-}$ mice could be rescued by PrP^C [8], suggesting that loss of PrP^C is necessary but not sufficient for inducing the neurodegeneration.

We and others independently identified a gene, *Prnd*, 16-kb downstream of the murine PrP gene, *Prnp* [6,9]. *Prnd* encodes a GPI-anchored PrP-like protein, named Doppel (Dpl), which shares 23% of amino acids with PrP [6,9] and exhibits similarity in conformation to the C-terminal globular domain of PrP^C [10]. Expression of *Prnd* is barely detectable in the brains of wild-type mice [11]. In contrast, in the ataxic *Prnp*$^{-/-}$ mice, *Prnd* was constitutively transcribed as chimeric mRNAs due to abnormal intergenic splicing [6,9]. These mRNAs contained the *Prnp* non-coding exons 1/2 at the 5′ terminus followed by the coding exon of *Prnd* with or without insertion of the intergenic exons [6,9]. As a consequence, Dpl was ectopically expressed in the brains of ataxic *Prnp*$^{-/-}$ mice under the control of the *Prnp* promoter [6,9]. In contrast, such chimeric mRNAs were undetectable in non-ataxic *Prnp*$^{-/-}$ mice [6,9]. Moore et al. [12] recently demonstrated that Zrch I *Prnp*$^{-/-}$ mice expressing transgenic Dpl under the control of the PrP promoter developed similar ataxia and degeneration, indicating a neurotoxic role of Dpl. The PrP promoter is very active in Purkinje cells, other neurons, and glial cells [13–15].

In this study, to further elucidate the mechanism of the neurodegeneration, we introduced Dpl transgenes (tg) under the control of a neuron- or Purkinje cell-specific promoter into mice with Zrch I *Prnp*$^{-/-}$,

* Corresponding author. Fax: +81-95-849-7060.
E-mail address: suehiros-ngs@umin.ac.jp (S. Sakaguchi).

0006-291X/$ - see front matter © 2004 Elsevier Inc. All rights reserved.
doi:10.1016/j.bbrc.2004.05.115

Prnp$^{+/-}$, or *Prnp*$^{+/+}$ background. We show here that the expression of Dpl in neurons or only in Purkinje cells themselves was sufficient for the degeneration, and that the neurotoxicity of Dpl was stoichiometrically antagonized by PrP^{C}.

Materials and methods

Mice. Ngsk and Zrch I *Prnp*$^{-/-}$ mice were generated as described previously [3,5]. Animals were cared for in accordance with Guidelines for Animal Experimentation of Nagasaki University.

Generation of transgenic mice. DNA consisting of part of intergenic exon 2 and the open reading frame (ORF) of murine Dpl was amplified by reverse transcriptase-polymerase chain reaction using total RNA extracted from the brains of Ngsk *Prnp*$^{-/-}$ mice with primer pairs of intex2-sense (5′-CCCGTCGACAAGCTTATGATGGAGTGGAGG TCGCTT-3′; underlined sequence represents the *Hin*dIII and *Sal*I recognition sites) and Dpl-antisense (5′-CCCGTCGACAAGCTT TTATTACTTCACAATGAACCAAAC-3′). The amplified DNA was digested with *Hin*dIII and inserted into a pNSE-EX 4 plasmid downstream of the ~4-kb genomic DNA of a rat neuron-specific enolase (NSE) gene [16], yielding the transgene NSE-Dpl. Additionally, only the Dpl ORF was amplified using primer pairs of Dpl-sense (5′-CCCGTCGACAAGCTTATGAAGAACCGGCTGGGTACA-3′) and -antisense, digested by *Sal*I, and cloned into a plasmid containing the genomic DNA derived from the Purkinje cell protein (PCP)-2 gene [17] to generate the transgene PCP2-Dpl. After removing the plasmid-derived sequence, the transgenes were injected into the zygotes of C57BL/6 mice to generate tg mice.

Western blotting. 10% (w/v) brain-homogenates were prepared in a buffer (150 mM NaCl, 50 mM Tris–HCl, pH 7.5, 0.5% Triton X-100, 0.5% sodium deoxycholate, and 1 mM EDTA). Ten micrograms of total proteins was electrophoresed on 12% SDS–polyacrylamide gel and electrically transferred to an Immobilon-P PVDF membrane (Millipore, MA, USA). The membrane was incubated with G-20, anti-Dpl polyclonal antibodies (Santa Cruz Biotechnology, CA, USA), and horseradish peroxidase-conjugated secondary antibody (Santa Cruz Biotechnology). Signals were visualized using the ECL system (Amersham Biosciences, NJ, USA).

In situ hybridization. In situ hybridization was performed as described elsewhere [9]. Briefly, brains were fixed in paraformaldehyde, embedded in paraffin, and sliced at 5 μm thickness. After deparaffinization, the sections were subjected to hybridization with cRNA probes labelled with digoxigenin (DIG)-UTP (Roche Diagnostics, Mannheim, Germany) in a hybridization buffer. Signals were detected by enzyme-linked immunosorbent assay using alkaline phosphatase-conjugated anti-DIG Fab fragments (1:500, Roche Diagnostics) and nitro blue tetrazolium/5-bromo-4-chloro-3-indolyl phosphate. The probes used for Dpl and inositol 1,4,5,-triphosphate receptor 1 (IP3R1) were derived from the ~1.1-kb Dpl ORF and the 664 bp PCR product corresponding to nucleotide 2823–3487 (Accession No. X15373s), respectively.

Results

Generation of tg mice expressing Dpl in neurons or Purkinje cells

The two constructs, termed NSE-Dpl and PCP2-Dpl, were designed to be expressed in all neurons or specifically in Purkinje cells, respectively (Figs. 1A and B), and injected into the zygotes of C57BL/6 mice, yielding three tg lines, tg(N-Dpl)25, 31, and 32 with NSE-Dpl and four tg lines, tg(P-Dpl)18, 26, 27, and 48 with PCP2-Dpl.

On Western blotting, all tg(N-Dpl) lines showed substantial Dpl in the cerebrum and cerebellum (Fig. 2A). In comparison with Ngsk *Prnp*$^{-/-}$ mice, the levels in tg(N-Dpl)25 mice were less than a quarter. The tg(N-Dpl)31 mice expressed about 2–3 times more in the cerebrum but the level in the cerebellum was about half. The highest expression was observed in tg(N-Dpl)32 mice at about 2–3 and 1–2 times more in the cerebrum and cerebellum, respectively. In situ hybridization of these mice gave the Dpl mRNA signals exclusively in neurons throughout the cerebrum and in Purkinje cells in the cerebellum (Fig. 2B). We failed to detect the Dpl mRNA in granule cells in the cerebellum, presumably due to the limited sensitivity of the assay.

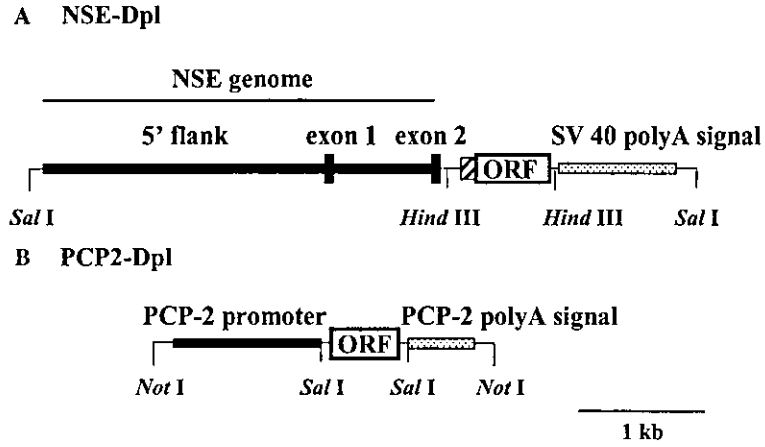

Fig. 1. Configurations of the NSE-Dpl and PCP2-Dpl transgenes. (A) In the NSE-Dpl transgene, the murine Dpl open reading frame (ORF) fused to the intergenic exon 2 at the 5′ terminus is transcribed from a neuron-specific enolase (NSE) promoter and terminates at the polyA signal of simian virus (SV) 40. (B) The PCP2-Dpl transgene consists of the Dpl ORF flanked by the sequences of the promoter and polyA signal derived from the Purkinje cell protein (PCP)-2 gene, a gene specifically expressed by Purkinje cells, at the 5′ and 3′ termini, respectively.

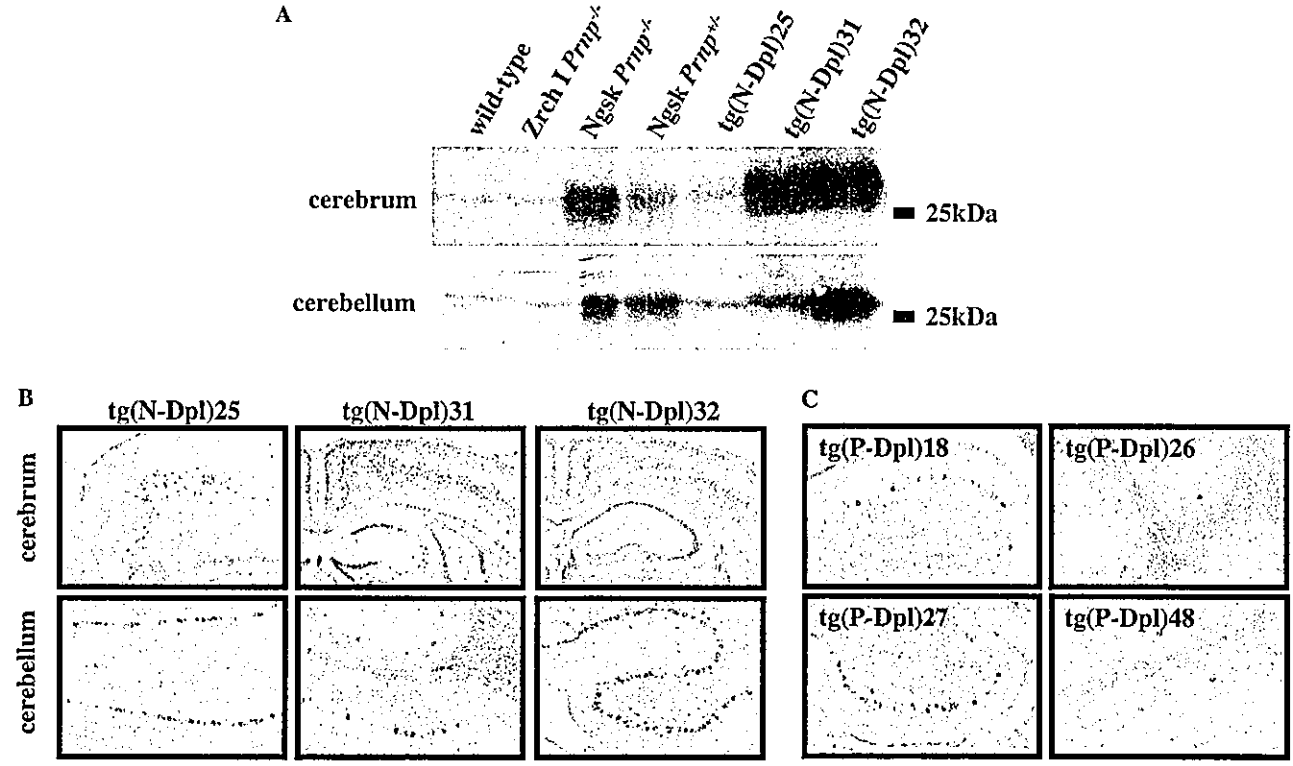

Fig. 2. (A) Western blotting of the cerebra and cerebella of different lines of tg(N-Dpl) mice together with wild-type, Zrch I *Prnp*$^{-/-}$, Ngsk *Prnp*$^{-/-}$, and Ngsk *Prnp*$^{+/-}$ mice with G-20, anti-Dpl polyclonal antibodies. In situ hybridization confirming the Dpl mRNA expression (represented by purple colors) in the cerebra and cerebella of tg(N-Dpl)25, 31, and 32 mice (B) and in the cerebella of tg(P-Dpl)18, 26, 27, and 48 mice (C). Original magnifications, 10× for the cerebrum and 50× for the cerebellum. (For interpretation of the references to color in this figure legend, the reader is referred to the web version of this paper.)

These signals were not co-localized with the immunoreactivity for glial fibrillary acidic protein, a specific marker for astrocytes (data not shown), strongly supporting the neuron-specific expression of Dpl in these tg mice.

Western blotting failed to detect Dpl in the cerebrum and cerebellum from all tg(P-Dpl) lines (data not shown). However, in situ hybridization of these mice visualized signals for Dpl mRNA in the Purkinje cells (Fig. 2C). The heavily stained Purkinje cells were evenly aligned throughout the cerebellar cortex of tg(P-Dpl)18 and 27 mice. Tg(P-Dpl)26 and 48 mice exhibited weak signals in most Purkinje cells but a few cells stained strongly. No signals were detectable in other cell types. The failed detection of Dpl by Western blotting was likely to be due to the highly limited expression of Dpl to the Purkinje cells of tg(P-Dpl) mice.

Dpl expressed by Purkinje cells causes ataxia and Purkinje cell death in Prnp$^{-/-}$ *mice*

Tg(N-Dpl)25 and 32 mice and tg(P-Dpl)26 and 27 mice were backcrossed with Zrch I *Prnp*$^{-/-}$ mice to generate each tg line of mice carrying the *Prnp*$^{-/-}$ alleles. No offspring with the *Prnp*$^{+/+}$ background, or founder mice, developed ataxia for up to at least 600 days after birth (Table 1). In contrast, all of the tg(N-Dpl)25 and 32 mice carrying the *Prnp*$^{-/-}$ genotype exhibited ataxia at 359 ± 52 and 58 ± 15 days, respectively (Table 1). The tg(P-Dpl)26 and 27 mice with the *Prnp*$^{-/-}$ background also developed ataxia at 268 ± 28 and 167 ± 13 days, respectively (Table 1). The times to the onset of ataxia in both types of tg mice were inversely correlated to the expression levels of Dpl in their brains, roughly estimated from the results of either Western blotting or in situ hybridization (Table 1).

We next examined the pathology of Purkinje cells of the ataxic tg mice by in situ hybridization with IP3R1, a marker for Purkinje cells. In the tg mice with the *Prnp*$^{+/+}$ alleles (data not shown) and the non-tg Zrch I *Prnp*$^{-/-}$ mice, Purkinje cells remained unaffected even at 694 days of age (Fig. 3g). In contrast, numbers of Purkinje cells were markedly decreased in aged Ngsk *Prnp*$^{-/-}$ mice (Fig. 3d). Ataxic tg(N-Dpl) and tg(P-Dpl) mice with the Zrch I *Prnp*$^{-/-}$ genotype exhibited similar loss of Purkinje cells (Figs. 3c, f, i, and k). No pathological changes were detectable in other cells, including granule cells. These results indicate that, in the absence of PrP^C, ectopic Dpl expressed by neurons or in Purkinje cells only causes degeneration of the cells.

Table 1
Summary of Dpl expression and onset of ataxia in tg(Dpl) mice

tg lines	Levels of Dpl[a]		Onset of ataxia [means ± SD days (ataxic/total mice)]		
	Cerebrum	Cerebellum	Zrch I *Prnp*$^{-/-}$	Zrch I *Prnp*$^{+/-}$	Zrch I *Prnp*$^{+/+}$
tg(N-Dpl)25	<1/4×	<1/4×	359 ± 52 (12/12)	495 ± 86 (6/20)	>600 (0/1)
tg(N-Dpl)31	2–3×	~1/2×	ND	ND	ND
tg(N-Dpl)32	2–3×	1–2×	58 ± 15 (10/10)	259 ± 48 (5/5)	>600 (0/10)
tg(P-Dpl)18	–	++	ND	ND	ND
tg(P-Dpl)26	–	+	268 ± 28 (8/8)	463 ± 81 (5/10)	>600 (0/4)
tg(P-Dpl)27	–	+++	167 ± 13 (4/4)	391 ± 108 (3/10)	>600 (0/1)
tg(P-Dpl)48	–	+	ND	ND	ND

SD, standard deviation; ND, not determined.
[a] The levels of Dpl expression are roughly determined by Western blotting in tg(N-Dpl) mice and by in situ hybridization in tg(P-Dpl) mice. –, not detectable; +, weakly expressed; ++, moderately expressed; and +++, strongly expressed.

PrP^C stoichiometrically antagonizes the neurotoxicity of Dpl

We examined the tg offspring hemizygous for Zrch I *Prnp* allele, *Prnp*$^{+/-}$. All tg(N-Dpl)32 mice with the *Prnp*$^{+/-}$ background developed ataxia at 259 ± 48 days after birth, and 6/20 tg(N-Dpl)25 mice showed similar symptoms at 495 ± 86 days on the *Prnp*$^{+/-}$ background (Table 1). 5/10 tg(P-Dpl)26 mice and 3/10 tg(P-Dpl)27 mice also became ataxic at 463 ± 81 and 391 ± 108 days, respectively, on the *Prnp*$^{+/-}$ background (Table 1). However, the onset of the ataxia in each line of tg mice with the *Prnp*$^{+/-}$ background was much prolonged, compared with that of the same line of mice with the *Prnp*$^{-/-}$ background (Table 1), indicating that, in contrast to Dpl, the time to ataxia onset is correlated to the

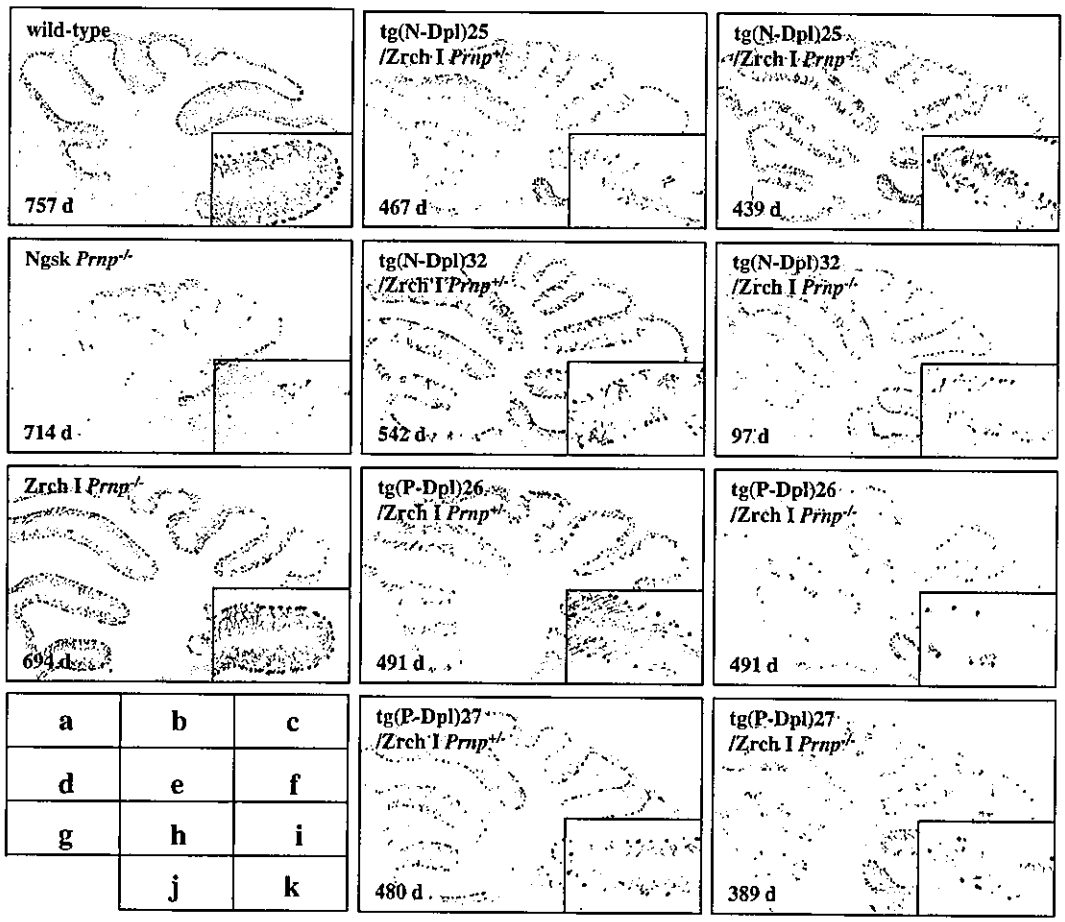

Fig. 3. Purkinje cell degeneration revealed by in situ hybridization with IP3R1 in the cerebella of ataxic tg(N-Dpl) and tg(P-Dpl) mice with the genetic background of Zrch I *Prnp*$^{+/-}$, and Zrch I *Prnp*$^{-/-}$. d, days. Magnifications, 10×. Inset magnification, 50×.

expression levels of PrP^C in the brains. Pathological examinations of Purkinje cells with in situ hybridization revealed that all ataxic tg mice with the *Prnp*$^{+/-}$ genotype showed massive degeneration of Purkinje cells (Figs. 3b, e, h, and j). These results indicate that PrP^C antagonizes the neurotoxicity of Dpl in a stoichiometric manner.

Discussion

In this study, we generated two types of Dpl-expressing tg mice, tg(N-Dpl) and tg(P-Dpl) mice. The former mice expressed Dpl specifically in neurons including Purkinje cells, and the latter expressed Dpl only in Purkinje cells. We showed here that both tg(N-Dpl) and tg(P-Dpl) mice developed ataxia with marked degeneration of Purkinje cells on the Zrch I *Prnp*$^{-/-}$ background, indicating that Dpl ectopically expressed by Purkinje cells themselves is toxic to the cells. Moreover, the neurodegeneration did not occur in both types of tg mice carrying the *Prnp*$^{+/+}$ alleles, reinforcing the idea that the functional antagonism of PrP^C against Dpl is crucially involved in the protection of the degeneration [18].

Neurodegeneration was observed only in Purkinje cells even in the brains of tg(N-Dpl) mice, in which Dpl was expressed by other neurons as well. Moore et al. [12] reported that in tg mice expressing Dpl, not only Purkinje cells but also hippocampal pyramidal cells and cerebellar granule cells were degenerative. These results suggest that although Purkinje cells are the most vulnerable to the toxicity of Dpl, Dpl could also exert deleterious effects on other neurons to a lesser extent by a common mechanism.

Consistent with the previous reports [7,12], the levels of ectopic Dpl in the brains of both tg(N-Dpl) and tg(P-Dpl) mice were inversely correlated to the time at onsets of ataxia, indicating the dose-dependent toxic effect of Dpl on Purkinje cells. In contrast to the complete protection by the *Prnp*$^{+/+}$ alleles, a single *Prnp* allele could partially rescue tg(N-Dpl) and tg(P-Dpl) mice from the Purkinje cell degeneration. Some tg mice with the Zrch I *Prnp*$^{+/-}$ background developed ataxia and Purkinje cell degeneration but much later than the corresponding line of mice with the Zrch I *Prnp*$^{-/-}$ background, indicating that PrP^C antagonizes the neurotoxicity of Dpl in a dose-dependent way. It is thus likely that the ratio of expression levels between PrP^C and ectopic Dpl in Purkinje cells is a determinant of the neurodegeneration.

It was recently reported that the targeted expression of PrPΔ32–134, lacking the N-terminal residues 32–134, to Purkinje cells of Zrch I *Prnp*$^{-/-}$ mice caused ataxia due to Purkinje cell degeneration [19,20]. PrPΔ32–134 lacks the octapeptide repeat and central hydrophobic region, but preserves the C-terminal residues with homology to Dpl. It is therefore very likely that Dpl and the truncated PrP could utilize the same or at least a similar molecular mechanism to execute their neurotoxicity on Purkinje cells. Interestingly, in contrast to PrPΔ32–134, PrPΔ23–88 has never shown neurotoxicity in Zrch I *Prnp*$^{-/-}$ mice, indicating that the residues between 88 and 134 are important to inhibit the neurotoxic potential of PrP^C [21]. This region, overlapping with the hydrophobic region, forms part of the binding sites for the heat shock protein, stress-inducible protein 1 [22], and the extracellular matrix constituent, glycosaminoglycans [23]. It would be of interest to examine the involvement of these associating molecules in the Purkinje cell degeneration in the ataxic *Prnp*$^{-/-}$ mice.

Acknowledgments

This was supported in part by a Research for Comprehensive Promotion of Study of Brain and a Grand-in-Aid for Scientific Research on Priority Areas—Advanced Brain Science Project—from the Ministry of Education, Culture, Sports, Science and Technology, Japan, and by a Research on Specific Diseases from the Ministry of Health, Labour and Welfare, Japan. We thank Dr. Patrick Tremblay and Professor Stanley B. Prusiner for providing Zrch I *Prnp*$^{-/-}$ mice and Professor Bruce Chesebro for a pNSE-EX 4 plasmid.

References

[1] S.B. Prusiner, Prions, Proc. Natl. Acad. Sci. USA 95 (1998) 13363–13383.
[2] B. Oesch, D. Westaway, M. Walchli, M.P. McKinley, S.B. Kent, R. Aebersold, R.A. Barry, P. Tempst, D.B. Teplow, L.E. Hood, et al., A cellular gene encodes scrapie PrP 27–30 protein, Cell 40 (1985) 735–746.
[3] H. Bueler, M. Fischer, Y. Lang, H. Bluethmann, H.P. Lipp, S.J. DeArmond, S.B. Prusiner, M. Aguet, C. Weissmann, Normal development and behaviour of mice lacking the neuronal cell-surface PrP protein, Nature 356 (1992) 577–582.
[4] J.C. Manson, A.R. Clarke, M.L. Hooper, L. Aitchison, I. McConnell, J. Hope, 129/Ola mice carrying a null mutation in PrP that abolishes mRNA production are developmentally normal, Mol. Neurobiol. 8 (1994) 121–127.
[5] S. Sakaguchi, S. Katamine, N. Nishida, R. Moriuchi, K. Shigematsu, T. Sugimoto, A. Nakatani, Y. Kataoka, T. Houtani, S. Shirabe, H. Okada, S. Hasegawa, T. Miyamoto, T. Noda, Loss of cerebellar Purkinje cells in aged mice homozygous for a disrupted PrP gene, Nature 380 (1996) 528–531.
[6] R.C. Moore, I.Y. Lee, G.L. Silverman, P.M. Harrison, R. Strome, C. Heinrich, A. Karunaratne, S.H. Pasternak, M.A. Chishti, Y. Liang, P. Mastrangelo, K. Wang, A.F. Smit, S. Katamine, G.A. Carlson, F.E. Cohen, S.B. Prusiner, D.W. Melton, P. Tremblay, L.E. Hood, D. Westaway, Ataxia in prion protein (PrP)-deficient mice is associated with upregulation of the novel PrP-like protein doppel, J. Mol. Biol. 292 (1999) 797–817.
[7] D. Rossi, A. Cozzio, E. Flechsig, M.A. Klein, T. Rulicke, A. Aguzzi, C. Weissmann, Onset of ataxia and Purkinje cell loss in PrP null mice inversely correlated with Dpl level in brain, EMBO J. 20 (2001) 694–702.
[8] N. Nishida, P. Tremblay, T. Sugimoto, K. Shigematsu, S. Shirabe, C. Petromilli, S.P. Erpel, R. Nakaoke, R. Atarashi, T. Houtani, M. Torchia, S. Sakaguchi, S.J. DeArmond, S.B. Prusiner, S.

Katamine, A mouse prion protein transgene rescues mice deficient for the prion protein gene from Purkinje cell degeneration and demyelination, Lab. Invest. 79 (1999) 689–697.
[9] A. Li, S. Sakaguchi, R. Atarashi, B.C. Roy, R. Nakaoke, K. Arima, N. Okimura, J. Kopacek, K. Shigematsu, Identification of a novel gene encoding a PrP-like protein expressed as chimeric transcripts fused to PrP exon 1/2 in ataxic mouse line with a disrupted PrP gene, Cell. Mol. Neurobiol. 20 (2000) 553–567.
[10] H. Mo, R.C. Moore, F.E. Cohen, D. Westaway, S.B. Prusiner, P.E. Wright, H.J. Dyson, Two different neurodegenerative diseases caused by proteins with similar structures, Proc. Natl. Acad. Sci. USA 98 (2001) 2352–2357.
[11] A. Li, S. Sakaguchi, K. Shigematsu, R. Atarashi, B.C. Roy, R. Nakaoke, K. Arima, N. Okimura, J. Kopacek, S. Katamine, Physiological expression of the gene for PrP-like protein, PrPLP/Dpl, by brain endothelial cells and its ectopic expression in neurons of PrP-deficient mice ataxic due to Purkinje cell degeneration, Am. J. Pathol. 157 (2000) 1447–1452.
[12] R.C. Moore, P. Mastrangelo, E. Bouzamondo, C. Heinrich, G. Legname, S.B. Prusiner, L. Hood, D. Westaway, S.J. DeArmond, P. Tremblay, Doppel-induced cerebellar degeneration in transgenic mice, Proc. Natl. Acad. Sci. USA 98 (2001) 15288–15293.
[13] S.J. DeArmond, W.C. Mobley, D.L. DeMott, R.A. Barry, J.H. Beckstead, S.B. Prusiner, Changes in the localization of brain prion proteins during scrapie infection, Neurology 37 (1987) 1271–1280.
[14] M. Moser, R.J. Colello, U. Pott, B. Oesch, Developmental expression of the prion protein gene in glial cells, Neuron 14 (1995) 509–517.
[15] D.R. Brown, A. Besinger, J.W. Herms, H.A. Kretzschmar, Microglial expression of the prion protein, Neuroreport 9 (1998) 1425–1429.
[16] R.E. Race, S.A. Priola, R.A. Bessen, D. Ernst, J. Dockter, G.F. Rall, L. Mucke, B. Chesebro, M.B. Oldstone, Neuron-specific expression of a hamster prion protein minigene in transgenic mice induces susceptibility to hamster scrapie agent, Neuron 15 (1995) 1183–1191.
[17] S. Vandaele, D.T. Nordquist, R.M. Feddersen, I. Tretjakoff, A.C. Peterson, H.T. Orr, Purkinje cell protein-2 regulatory regions and transgene expression in cerebellar compartments, Genes Dev. 5 (1991) 1136–1148.
[18] A. Behrens, A. Aguzzi, Small is not beautiful: antagonizing functions for the prion protein PrP(C) and its homologue Dpl, Trends Neurosci. 25 (2002) 150–154.
[19] D. Shmerling, I. Hegyi, M. Fischer, T. Blattler, S. Brandner, J. Gotz, T. Rulicke, E. Flechsig, A. Cozzio, C. von Mering, C. Hangartner, A. Aguzzi, C. Weissmann, Expression of amino-terminally truncated PrP in the mouse leading to ataxia and specific cerebellar lesions, Cell 93 (1998) 203–214.
[20] E. Flechsig, I. Hegyi, R. Leimeroth, A. Zuniga, D. Rossi, A. Cozzio, P. Schwarz, T. Rulicke, J. Gotz, A. Aguzzi, C. Weissmann, Expression of truncated PrP targeted to Purkinje cells of PrP knockout mice causes Purkinje cell death and ataxia, EMBO J. 22 (2003) 3095–3101.
[21] R. Atarashi, N. Nishida, K. Shigematsu, S. Goto, T. Kondo, S. Sakaguchi, S. Katamine, Deletion of N-terminal residues 23–88 from prion protein (PrP) abrogates the potential to rescue PrP-deficient mice from PrP-like protein/doppel-induced neurodegeneration, J. Biol. Chem. 278 (2003) 28944–28949.
[22] S.M. Zanata, M.H. Lopes, A.F. Mercadante, G.N. Hajj, L.B. Chiarini, R. Nomizo, A.R. Freitas, A.L. Cabral, K.S. Lee, M.A. Juliano, E. de Oliveira, S.G. Jachieri, A. Burlingame, L. Huang, R. Linden, R.R. Brentani, V.R. Martins, Stress-inducible protein 1 is a cell surface ligand for cellular prion that triggers neuroprotection, EMBO J. 21 (2002) 3307–3316.
[23] R.G. Warner, C. Hundt, S. Weiss, J.E. Turnbull, Identification of the heparan sulfate binding sites in the cellular prion protein, J. Biol. Chem. 277 (2002) 18421–18430.

Cellular and Molecular Neurobiology, Vol. 24, No. 2, April 2004 (© 2004)

Uptake and Efflux of Quinacrine, a Candidate for the Treatment of Prion Diseases, at the Blood-Brain Barrier

Shinya Dohgu,[1,2] Atsushi Yamauchi,[2] Fuyuko Takata,[2] Yasufumi Sawada,[1] Shun Higuchi,[1] Mikihiko Naito,[3] Takashi Tsuruo,[3] Susumu Shirabe,[4] Masami Niwa,[4] Shigeru Katamine,[4] and Yasufumi Kataoka[2,5]

Received April 7, 2003; accepted May 22, 2003

SUMMARY

1. A clinical trial of quinacrine in patients with Creutzfeldt–Jakob disease is now in progress. The permeability of drugs through the blood–brain barrier (BBB) is a determinant of their therapeutic efficacy for prion diseases. The mechanism of quinacrine transport across the BBB was investigated using mouse brain endothelial cells (MBEC4).

2. The permeability of quinacrine through MBEC4 cells was lower than that of sodium fluorescein, a BBB-impermeable marker. The basolateral-to-apical transport of quinacrine was greater than its apical-to-basolateral transport. In the presence of P-glycoprotein (P-gp) inhibitor, cyclosporine or verapamil, the apical-to-basolateral transport of quinacrine increased. The uptake of quinacrine by MBEC4 cells was enhanced in the presence of cyclosporine or verapamil.

3. Quinacrine uptake was highly concentrative, this event being carried out by a saturable and carrier-mediated system with an apparent K_m of 52.1 μM. Quinacrine uptake was insensitive to Na^+-depletion and changes in the membrane potential and sensitive to changes in pH. This uptake was decreased by tetraethylammonium and cimetidine, a substrate and an inhibitor of organic cation transporters, respectively.

4. These findings suggest that quinacrine transport at the BBB is mediated by the efflux system (P-gp) and the influx system (organic cation transporter-like machinery).

KEY WORDS: quinacrine; blood–brain barrier; mouse brain endothelial cells; P-glycoprotein; organic cation transporter; Creutzfeldt–Jakob disease.

INTRODUCTION

Prion diseases including Creutzfeldt–Jakob disease (CJD) are progressive, fatal neurodegenerative diseases induced by conformational changes in prion protein (PrP) in

[1] Department of Medico-Pharmaceutical Sciences, Graduate School of Pharmaceutical Sciences, Kyushu University, Fukuoka, Japan.
[2] Department of Pharmaceutical Care and Health Sciences, Faculty of Pharmaceutical Sciences, Fukuoka University, Fukuoka, Japan.
[3] Institute of Molecular and Cellular Biosciences, University of Tokyo, Tokyo, Japan.
[4] Nagasaki University Graduate School of Biomedical Sciences, Nagasaki, Japan.
[5] To whom correspondence should be addressed at Department of Pharmaceutical Care and Health Sciences, Faculty of Pharmaceutical Sciences, Fukuoka University, 8-19-1 Nanakuma, Jonan-ku, Fukuoka 814-0180, Japan; e-mail: ykataoka@cis.fukuoka-u.ac.jp.

0272-4340/04/0400-0205/0 © 2004 Plenum Publishing Corporation

the central nervous system. It has been reported that quinacrine, an antimalarial drug, could rapidly eradicate production of the disease-associated and protease-resistant isoform of the prion protein (PrP^{SC}) in vitro (Korth *et al.*, 2001). A clinical trial of quinacrine has started at the Department of Neurology, Faculty of Medicine, Fukuoka University and the Department of Neurology, Faculty of Medicine, Nagasaki University. A transient improvement was observed in CJD patients (Follette, 2003).

The members of organic cation transporter (OCT) family include OCT1 (Grundemann *et al.*, 1994), OCT2 (Okuda *et al.*, 1996), OCT3 (Kekuda *et al.*, 1998), novel organic cation transporter (OCTN)1 (Tamai *et al.*, 1997), OCTN2 (Wu *et al.*, 1998), and OCTN3 (Tamai *et al.*, 2000). The tissue distribution patterns of the OCT family are dependent on the animal species. In the human and rat brain, OCT2 mRNA (Koepsell, 1998), OCTN1 mRNA (Tamai *et al.*, 1997; Wu *et al.*, 2000), and OCTN2 mRNA (Wu *et al.*, 1998, 1999) have been detected. OCTN1 and OCTN2 are expressed in the mouse brain (Tamai *et al.*, 2000). Immortalized rat brain endothelial cells (RBE4) express OCTN2 (Friedrich *et al.*, 2003). OCTN1 and OCTN2 are structurally much more closely related to each other than to OCT1, OCT2, and OCT3 (Wu *et al.*, 2000). Quinacrine is an organic cation and an organic base. The entry of organic cations such as choline into the brain occurs via transport systems present in the blood brain barrier (BBB) (Friedrich *et al.*, 2001; Sawada *et al.*, 1999). The transport of L-carnitine was mediated by OCTN2 in RBE4 cells (Friedrich *et al.*, 2003). Quinacrine inhibited tetraethylammonium (TEA) transport in MDCK cells expressing rat OCT2 (Sweet and Pritchard, 1999).

The BBB permeability of quinacrine is a determinant of its therapeutic efficacy for CJD. Quinacrine is known to pass through the BBB (Korth *et al.*, 2001), although the extent of quinacrine penetration into the brain and the mechanism involved in quinacrine transport across the BBB remain obscure. In this study, we investigated the properties of quinacrine transport into the brain using mouse brain capillary endothelial cells (MBEC4).

MATERIALS AND METHODS

Materials

Quinacrine dihydrochloride and sodium azide (NaN_3) were purchased from Tokyo Kasei Kogyo (Tokyo, Japan) and Kishida Kagaku (Osaka, Japan), respectively. N-Methylglucamine, 2,4-dinitrophenol (DNP), carbonyl cyanide *p*-(trifluoromethoxy) phenylhydrazone (FCCP), valinomycin, amiloride, tetraethylammonium (TEA), cimetidine, and verapamil were purchased from Sigma (St. Louis, MO). Cyclosporine was kindly supplied by Novartis (Basel, Switzerland). All other chemicals were commercial products of reagent grade.

Cell Culture

MBEC4 cells isolated from BALB/c mice brain cortices and immortalized by SV40-transformation (Tatsuta *et al.*, 1992) were cultured in Dulbecco's modified Eagle's medium (DMEM) (GIBCO BRL, Life Technologies, Grand Island, NY)

supplemented with 10% fetal bovine serum, 100 units/mL penicillin, and 100 μg/mL streptomycin in a humidified atmosphere of 5% CO_2/95% air at 37°C. For the transport experiments, MBEC4 cells (42,000 cells/cm^2) were plated into the collagen-coated polycarbonate membrane (1.0 cm^2, 3.0-μm pore size) of the Transwell^{TM} insert (12-well type) (Costar, MA). For the cellular uptake experiments, cells were seeded at a density of 21,000 cells/cm^2 on 4- or 24-well multi dishes (Nunc, Roskilde, Denmark). MBEC4 cells were cultured for 3 days and then used for the following experiments. MBEC4 cells show both general brain endothelial and specific BBB characteristics including the expression of P-glycoprotein (P-gp) (Tatsuta *et al.*, 1992, 1994).

Transcellular Transport of Quinacrine Across MBEC4 Cells

To initiate the transport experiments, the medium was removed and cells were washed three times with Krebs-Ringer buffer (118 mM NaCl, 4.7 mM KCl, 1.3 mM $CaCl_2$, 1.2 mM $MgSO_4$, 1.0 mM NaH_2PO_4, 25 mM $NaHCO_3$, 11 mM D-glucose, pH 7.4). Krebs-Ringer buffer was applied on the outside of the insert in the well (abluminal side) (1.5 mL) and the luminal side of the insert (0.5 mL). Krebs-Ringer buffer containing 50–200 μM quinacrine (MW 473) or 100 μM sodium fluorescein (Na-F) (MW 376), a paracellular transport marker, was loaded on the luminal or abluminal side of the insert. Samples (0.5 mL) were removed from the luminal or abluminal chamber at 10, 20, 30, and 60 min and immediately replaced with fresh Krebs-Ringer buffer. The quinacrine concentration in the samples was determined using a multiwell fluorometer (Ex(λ) 450 nm; Em(λ) 530 nm) (CytoFluor Series 4000, PerSeptive Biosystems, Framingham, MA). Aliquots (5 μL) from the samples were mixed with 200 μL of Krebs-Ringer buffer and then the concentration of Na-F was measured (Ex(λ) 485 nm; Em(λ) 530 nm). Permeability coefficient and clearance were calculated according to the method described by Dehouck *et al.* (1992). Clearance was expressed as μL of tracer diffusing from the luminal to the abluminal chambers and was calculated from the initial concentration of tracer in the luminal chamber and the final concentration of tracer in the abluminal chamber: *Clearance* (μL) = $[C]_A \times V_A/[C]_L$ where $[C]_L$ is the initial luminal tracer concentration, $[C]_A$ is the abluminal tracer concentration, and V_A is the volume of the abluminal chamber. During the 60-min period of the experiment, the clearance volume increased linearly with time. The average volume cleared was plotted versus time, and the slope was estimated by linear regression analysis. The slope of clearance curves for the MBEC4 monolayer was denoted PS_{app}, where PS is the permeability $\times$ surface area product (in μL per min). The slope of the clearance curve with the control membrane was denoted $PS_{membrane}$. The real PS value for the MBEC4 monolayer (PS_{trans}) was calculated from $1/PS_{app} = 1/PS_{membrane} + 1/PS_{trans}$. The PS_{trans} values were divided by the surface area of the Transwell^{TM} inserts to generate the permeability coefficient (P_{trans}, in cm per min).

Cellular Uptake of Quinacrine by MBEC4 Cells

For the uptake experiments, MBEC4 cells were washed three times with uptake buffer (143 mM NaCl, 4.7 mM KCl, 1.3 mM $CaCl_2$, 1.2 mM $MgSO_4$, 11 mM D-glucose,

10 mM HEPES, pH 7.4) and incubated with 0.5 mL of the uptake buffer containing quinacrine (1–200 μM) at 37°C for 1–120 min. After incubation, the buffer was removed and cells were washed three times with ice-cold phosphate-buffered saline. The cells were solubilized with 250 μL of 1 N NaOH. Aliquots of the cell solution were removed for protein assay according to the method of Bradford using a Bio-Rad protein assay kit (Bio-Rad Laboratories, Hercules, CA) (Bradford, 1976). Aliquots (200 μL) of the cell solution were neutralized with 200 μL of 1 N HCl and then sample fluorescence was measured (Ex(λ) 450 nm; Em(λ) 530 nm). Quinacrine uptake is expressed as the cell-to-medium ratio (quinacrine amounts in the cells/quinacrine concentration in the medium).

Estimation of Kinetic Parameters

The kinetic parameters for quinacrine uptake by MBEC4 cells were calculated by fitting the uptake rate (V) to the following equation: $V = (V_{max} \times S)/(K_m + S) + P_{dif} \times S$ where V_{max} is the maximum uptake rate of quinacrine (nmol/15 min/mg protein), S is the quinacrine concentration in the medium (μM), K_m is the Michaelis–Menten constant (μM), P_{dif} is the first-order constant for the nonsaturable component (μL/15 min/mg protein). Curve fitting was performed by the nonlinear least-squares regression program, MULTI (Yamaoka *et al.*, 1981).

Detection of OCTN1 mRNA

Total RNA from MBEC4 cells was extracted using TRIZOL™ reagent (Invitrogen, Carlsbad, CA). The primer pair used in the reverse transcription-polymerase chain reaction (RT-PCR) was designed based on the nucleotide sequence of the mouse OCTN1 transporter. The upper primer was 5′-CCTGTTCTGTGTTCCCC-TGT-3′ and the lower primer was 5′-GGTTATGGTGGCAATGTTCC-3′. The expected size of the RT-PCR product, predicted from the positions of the primers, was 232 bp. A SuperScript One-Step RT-PCR system (Invitrogen) was used for reverse transcription of RNA, and OCTN1 cDNA were amplified by PCR. Amplification was performed in a DNA thermal cycler (PC707; ASTEC, Fukuoka, Japan) according to the following protocol: cDNA synthesis for 30 min at 50°C, predenaturation for 2 min at 94°C; 40 cycles of denaturation for 30 s at 94°C, primer annealing for 30 s at 57°C, and polymerization for 30 s at 70°C; and final extension for 5 min at 72°C. Each 10 μL of PCR product was analyzed by electrophoresis on a 3% agarose (Sigma) gel with ethidium bromide staining. The gels were photographed under UV light using a DC290 Zoom digital camera (Kodak, Rochester, New York).

Statistical Analysis

The results are expressed as means ± SEM. Statistical analysis was performed using the Student's unpaired t test. The differences between means were considered to be significant when P values were less than 0.05.

RESULTS

The MBEC4 permeability coefficient of quinacrine dose-dependently increased from $0.58 \pm 0.025 \times 10^{-3}$ to $2.1 \pm 0.15 \times 10^{-3}$ cm/min, when the quinacrine concentration was increased from 50 to 200 μM. The MBEC4 permeability coefficient of quinacrine (100 μM) was significantly lower than that of Na-F (Fig. 1(A)). Permeability coefficients of the basolateral-to-apical transport of quinacrine and Na-F were $1.1 \pm 0.054 \times 10^{-3}$ and $1.5 \pm 0.17 \times 10^{-3}$ cm/min, respectively, while those of the apical-to-basolateral transport were $0.66 \pm 0.023 \times 10^{-3}$ and $1.5 \pm 0.25 \times 10^{-3}$ cm/min, respectively. The basolateral-to-apical transport of quinacrine was significantly higher than that in the opposite direction of transport (Fig. 1(B)). Cyclosporine (10 μM) and verapamil (20 μM) significantly increased the permeability coefficients of the apical-to-basolateral transport of quinacrine from $0.66 \pm 0.023 \times 10^{-3}$ to $1.15 \pm 0.056 \times 10^{-3}$ cm/min and from $0.57 \pm 0.034 \times 10^{-3}$ to $1.02 \pm 0.080 \times 10^{-3}$ cm/min, respectively (Fig. 1(C)).

Quinacrine uptake by MBEC4 cells was time-dependent and reached to the peak at 30 min after the exposure. The cell-to-medium ratio of quinacrine uptake was $2.37 \pm 0.18 \times 10^3$ μL/mg protein at 1 min after the exposure (Fig. 2(A)). Taking the finding that the cell volume of MBEC4 cells is approximately 3 μL/mg protein (Sawada *et al.*, 1999) into consideration, quinacrine is found to be extensively concentrated in MBEC4 cells. To determine whether this apparent concentrative uptake occurs due to only passive entry followed by intracellular binding, MBEC4 cells were treated with 0.015% Triton X for 10 min (Chan *et al.*, 1998). This treatment significantly reduced quinacrine uptake by 30–40% in the period between 30 and 60 min after the addition of quinacrine (Fig. 2(B)). These findings demonstrated that the apparent concentrative accumulation of quinacrine is not due only to passive entry followed by intracellular binding, because quinacrine, when actively accumulated in MBEC4 cells against a concentration gradient and unbound to the binding sites, leaks from cells into the external media through the permeabilized plasma membrane. The initial rate of quinacrine uptake by MBEC4 cells became saturated at 15-min after the exposure to quinacrine (1–200 μM) (Fig. 2(C)). Analysis of these data indicated the involvement of two transport processes (saturable carrier-mediated and nonsaturable system) in quinacrine uptake by MBEC4 cells. The parameters obtained by kinetic analysis were as follows; $V_{max} = 218 \pm 5.4$ nmol/15 min/mg protein, $K_m = 52.1 \pm 1.7$ μM, and passive permeability constant (P_{dif}) $= 94.3 \pm 1.7$ μL/15 min/mg protein.

Quinacrine uptake during a 15-min period was decreased by preincubation of the cells for 10 min with the metabolic inhibitors, NaN_3 (10 mM), DNP (1 mM), and FCCP (10 μM) (Table I). When the experiment was performed at 4°C, quinacrine uptake was reduced (Table I). This uptake was not affected by replacement of the external sodium with N-methylglucamine (Table I) or by changing the external potassium concentration (4.32 ± 0.09, 4.36 ± 0.19, and $4.62 \pm 0.25 \times 10^3$ μL/mg protein at 0, 4.7, and 100 mM of K^+, respectively) (Fig. 3(A)). Pretreatment of MBEC4 cells for a 10-min period with 10 μM of valinomycin, a K^+ ionophore, did not affect quinacrine uptake (Table I). This uptake was elevated from 1.54 ± 0.04 to $4.56 \pm 0.14 \times 10^3$ μL/mg protein by elevating the external pH from 6.4 to 8.4

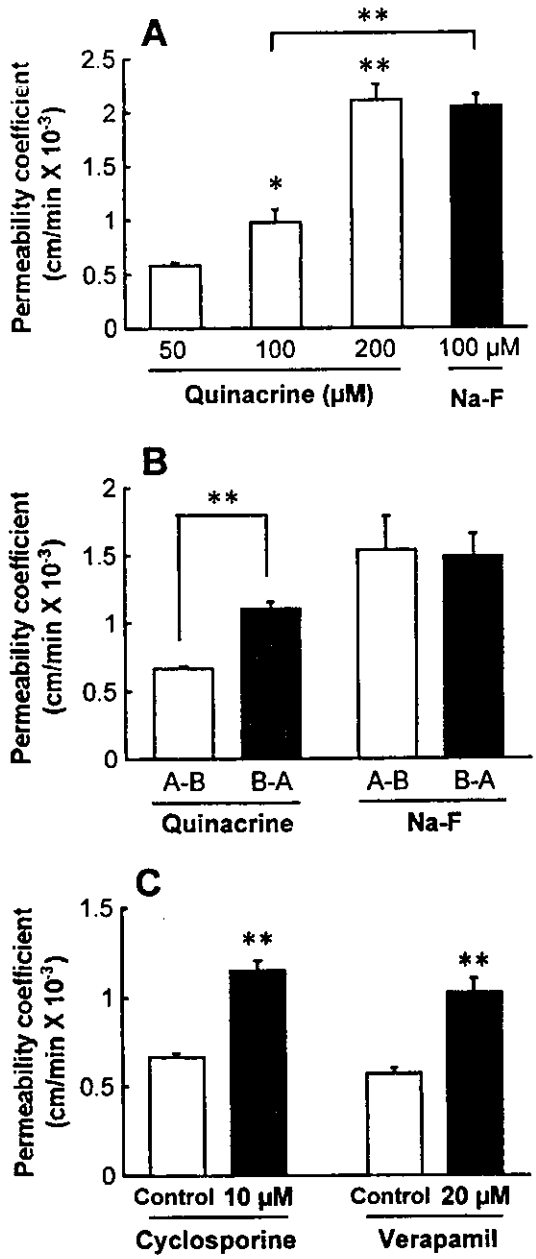

Fig. 1. Characteristics of quinacrine permeability through the MBEC4 monolayer. Panel (A), the permeability coefficients of quinacrine (50–200 μM) or Na-F (100 μM) through the MBEC4 monolayer. Panel (B), the permeability coefficients for the apical-to-basolateral ((A)–(B)) and basolateral-to-apical ((B)–(A)) transport of 100 μM quinacrine and 100 μM Na-F across the MBEC4 monolayer. (A)–(B) and (B)–(A) represent the blood-to-brain and brain-to-blood flux, respectively. Panel (C), the effects of 10 μM cyclosporine and 20 μM verapamil on the apical-to-basolateral transport of 100 μM quinacrine through the MBEC4 monolayer. The permeability coefficient of quinacrine was measured in the presence or absence of each drug. Values are means ± SEM. ($n = 3$–4 (A), 8 ((B), (C))). * $P < 0.05$ and ** $P < 0.01$; significant difference from the MBEC4 monolayer treated with 50μM quinacrine (A), the opposite direction (B), and the corresponding control (C).

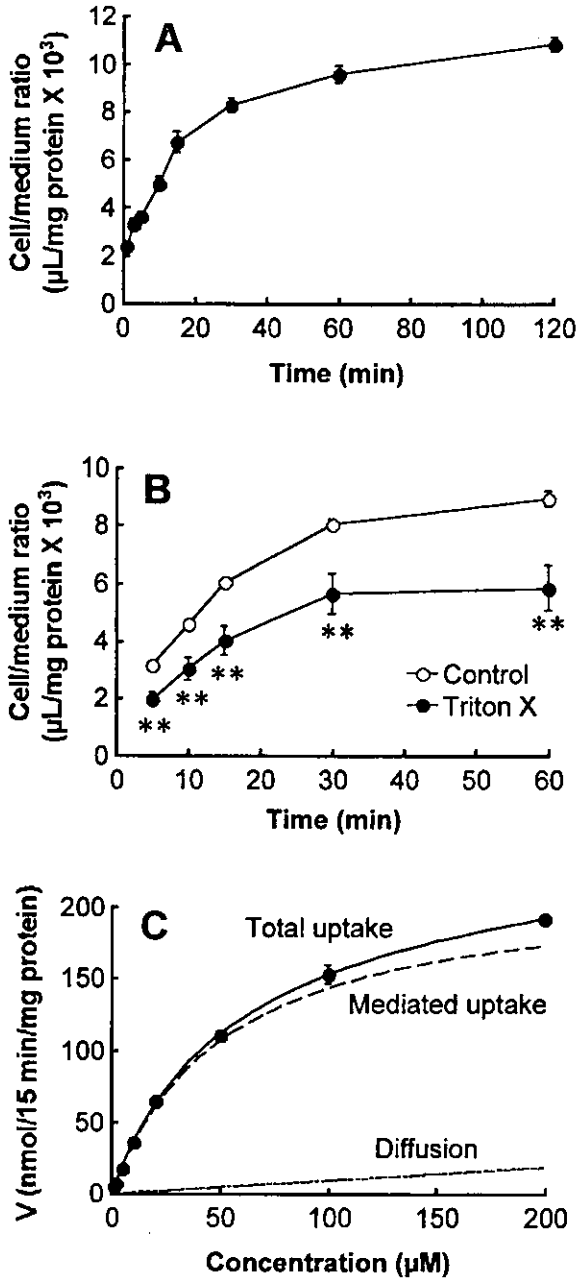

Fig. 2. Characteristics of quinacrine uptake by MBEC4 cells. Panel (A), time course of quinacrine (1 μM) uptake by MBEC4 cells. Panel (B), changes in the quinacrine (1 μM) uptake by MBEC4 cells exposed to 0.015% Triton X for 10 min before the uptake experiment. Panel (C), concentration-dependence of quinacrine uptake by MBEC4 cells. Initial uptake rates at various concentrations of quinacrine (1–200 μM) were measured at 37°C for 15 min. Curves for total, mediated, and diffusive uptake were drawn using the parameters obtained from nonlinear regression analysis (MULTI). Each point represents the mean ± SEM. ($n = 4$–20).** $P < 0.01$; significant difference from the control.

Table I. Effects of Various Compounds and Sodium-Replacement on Uptake of Quinacrine (1 μM) by MBEC4 Cells

Condition	Concentration	Cell/medium ratio (% of control)
NaN_3	10 mM	$67.2 \pm 3.03^{a,**}$
DNP	1 mM	$70.2 \pm 1.79^{a,**}$
4°C		$18.6 \pm 2.22^{a,**}$
FCCP	10 μM	$77.4 \pm 2.49^{a,**}$
Valinomycin	10 μM	97.2 ± 4.22^{a}
Amiloride	1 mM	97.4 ± 3.16^{a}
Tetraethylammonium	1 mM	$88.0 \pm 2.95^{b,**}$
	5 mM	$84.3 \pm 2.93^{b,**}$
	10 mM	$75.4 \pm 4.15^{b,**}$
Cimetidine	1 mM	$81.3 \pm 5.56^{c,**}$
	5 mM	$57.8 \pm 1.70^{c,**}$
	10 mM	$36.8 \pm 1.61^{c,**}$
Na^+ replacement with N-methylglucamine		104 ± 2.87^{d}

[a]MBEC4 cells were preincubated with NaN_3, DNP, FCCP, valinomycin, or amiloride for 10 min. Control values were $4.9 \pm 0.42 \times 10^3$ μL/mg protein. [b,c]Quinacrine uptake was measured by incubating MBEC4 cells with TEA or cimetidine. Control values were 4.1 ± 0.19 and $5.2 \pm 0.19 \times 10^3$ μL/mg protein, respectively.

[d]For investigation of the sodium dependency, quinacrine uptake was measured where Na^+ in the uptake buffer was replaced by N-methylglucamine. Control values were $3.6 \pm 0.22 \times 10^3$ μL/mg protein. Quinacrine uptake was measured at 37°C for 15 min. Values are expressed as % of control. Values are shown as means ± SEM ($n = 4$–20).

$^{**}P < 0.01$; significant difference from the control.

(Fig. 3(B)). These findings demonstrated that quinacrine uptake by MBEC4 cells was pH-dependent. Pretreatment with 10 mM of NaN_3 inhibited quinacrine uptake at each pH used (Table II). Quinacrine uptake was not affected by 1 mM of amiloride (Table I). Therefore, quinacrine uptake was found to be unaffected by Na^+/H^+

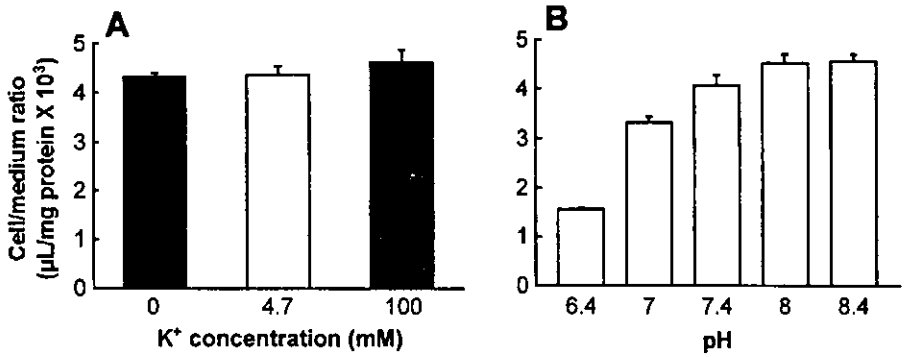

Fig. 3. Effects of the membrane potential (A) and pH (B) on the uptake of quinacrine (1 μM) by MBEC4 cells. Panel (A), effects of various concentrations of external potassium on quinacrine uptake: 0 mM (hyperpolarized), 4.7 mM (control), or 100 mM (depolarized). Panel (B), effects of various pH of the medium on quinacrine uptake. Quinacrine uptake was measured at 37°C for 15 min. Values are expressed as the cell-to-medium ratios. Values are shown as means ± SEM. ($n = 12$).

Table II. Effect of ATP Depletion on the Uptake of Quinacrine (1 μM) by MBEC4 Cells

	Cell/medium ratio (μL/mg protein $\times 10^3$)	
pH	Normal	ATP-depletion
6.4	1.61 ± 0.02	1.36 ± 0.03**
7.0	3.53 ± 0.14	3.28 ± 0.10
7.4	3.95 ± 0.32	3.20 ± 0.33*
8.0	4.71 ± 0.35	3.87 ± 0.30
8.4	4.77 ± 0.19	3.82 ± 0.22*

MBEC4 cells were preincubated with 10 mM NaN_3 for 10 min (ATP depletion). Quinacrine uptake was measured at 37°C for 15 min. Values are shown as means ± SEM ($n = 3$–8).
* $P < 0.05$, ** $P < 0.01$; significant difference from the control.

exchange. The effects of organic cations and P-gp inhibitors on quinacrine uptake were investigated. The organic cations including TEA (1-10 mM) and cimetidine (1–10 mM) significantly reduced quinacrine uptake by 12–25% and 19–65%, respectively (Table I). In the presence of cyclosporine (10 μM) or verapamil (20 μM), quinacrine uptake under the steady-state significantly increased by about 10% (Fig. 4).

To provide molecular evidence for the expression of OCTN1 in MBEC4 cells, RT-PCR was carried out (Fig. 5). With a primer pair specific for mouse OCTN1, RT-PCR with mRNA obtained from MBEC4 cells yielded a single product. The size of this product was the same as that expected from the primer positions in mouse OCTN1.

DISCUSSION

The BBB permeability coefficient of quinacrine, a candidate for the treatment of CJD, was much lower than that of Na-F, a BBB-impermeable marker, suggesting that

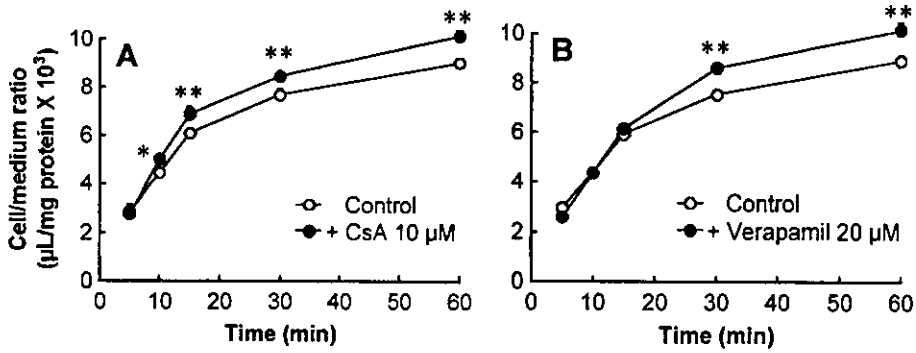

Fig. 4. Effects of 10 μM cyclosporine (A) and 20 μM verapamil (B) on uptake of quinacrine (1 μM) by MBEC4 cells. Quinacrine uptake was measured at 37°C in the absence and presence of cyclosporine or verapamil. Values are expressed as the cell-to-medium ratios. Values are shown as means ± SEM. ($n = 8$).

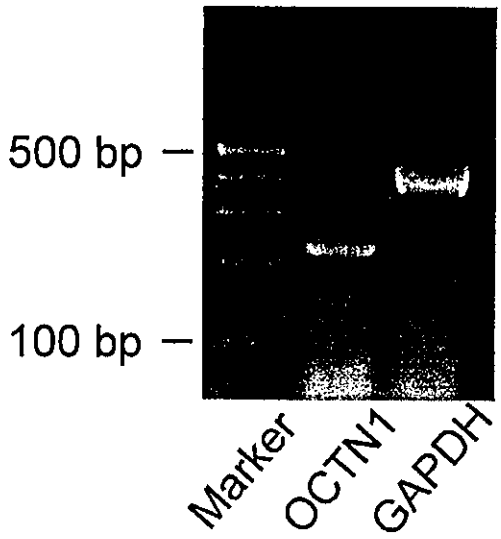

Fig. 5. Photograph showing OCTN1 expression in MBEC4 cells by RT-PCR. RNA samples from MBEC4 cells were used for RT-PCR with primer pairs specific for mouse OCTN1.

the permeability of quinacrine into the brain through the BBB is extremely low. To determine which machinery is involved in the low permeability of quinacrine across the BBB, we investigated the polarity of transcellular transport of quinacrine and the effects of P-gp inhibitors (cyclosporine and verapamil) on the BBB permeability of quinacrine. The basolateral-to-apical (brain-to-blood) transport of quinacrine across MBEC4 monolayer was greater than quinacrine transport in the opposite direction (Fig. 1(B)). Cyclosporine and verapamil increased the apical-to-basolateral (blood-to-brain) transport of quinacrine (Fig. 1(C)). Quinacrine uptake by MBEC4 cells under the steady-state was significantly increased by cyclosporine and verapamil (Fig. 4). These findings indicate the possible involvement of P-gp in the efflux transport of quinacrine. P-gp largely contributes to multidrug-resistance of the BBB in an ATP-dependent manner. This study provided controversial evidence that metabolic inhibitors or incubation at low temperature decreased quinacrine uptake (Table I). Quinacrine was actively and concentratively accumulated in MBEC4 cells. A large part of quinacrine is probably taken up via the saturable system, although quinacrine uptake was shown to have both saturable and nonsaturable pathways (Fig. 2(C)). Uptake of quinacrine by choroid plexus cells was organic cation-specific and energy-dependent (Miller *et al.*, 1999). In light of these findings, P-gp (an efflux system) and other influx transport system(s) are considered to mediate quinacrine transport into the brain.

We elucidated a role of the known organic cation transporters (OCT1, OCT2, OCT3, OCTN1, and OCTN2), and the specificity or driving force of those transporters in mediating quinacrine uptake by MBEC4 cells. Quinacrine uptake was significantly inhibited by various organic cations including TEA and cimetidine, which are known to be a substrate and an inhibitor of the organic cation transporters, respectively. Quinacrine uptake was insensitive to changes in the membrane potential (Fig. 3(A)) and strongly inhibited by lowering the external pH (Fig. 3(B)). These characteristics are distinct from those of the OCT1, OCT2, and OCT3, all of which

are dependent on the membrane potential (Gorboulev *et al.*, 1997; Grundemann *et al.*, 1994; Kekuda *et al.*, 1998). Considering quinacrine is an organic base, the pH-related decrease in quinacrine uptake may have resulted from an increase in the concentration of ionized quinacrine according to the pH partition theory. However, our data showing that quinacrine uptake by MBEC4 cells at each pH was inhibited by NaN_3 (Table II) suggest that a pH-sensitive transport system is involved in quinacrine uptake. Transport of quinacrine increased by elevating the outward H^+ gradient across the membrane. This finding indicates that quinacrine may be transported through MBEC4 cells by an H^+/quinacrine antiport. The activity of H^+/organic cation antiporter is regulated by pH or H^+ gradient as the driving force (Maegawa *et al.*, 1988). The H^+ gradient is formed by Na^+/H^+ exchange in the vicinity of the apical membrane of brain endothelial cells (Ennis *et al.*, 1996). The Na^+/H^+ exchange is, however, unlikely to participate in quinacrine uptake by MBEC4 cells, since Na^+-depletion and amiloride failed to reduce quinacrine uptake (Table I). OCTN1 is Na^+-independent organic cation transporter (Wu *et al.*, 2000). OCTN2 mediates uptake of L-carnitine and several organic cations in an Na^+-coupled and Na^+-independent manner, respectively (Wu *et al.*, 1999). OCTN1 is a pH-dependent organic cation transporter presumably energized by a proton antiport mechanism (Yabuuchi *et al.*, 1999). The characteristics of quinacrine transport obtained in this study are similar to those of OCTN1. Mouse OCTN1 is distributed in the brain, heart, and liver, and strongly expressed in the kidney (Tamai *et al.*, 2000). RT-PCR analysis of MBEC4 cells demonstrated the expression of OCTN1 (Fig. 5). Therefore, OCTN1 is suggested to be a potential transporter mediating quinacrine uptake by MBEC4 cells.

The BBB permeability of quinacrine was extremely low, although quinacrine was rapidly transported into the brain endothelial cells by the apical pH-dependent transport system. A weak organic base binds to a variety of polyanions including RNA, DNA, and ATP, and accumulates in the acidic intracellular compartments (Miller *et al.*, 1999). Quinacrine is distributed in the nucleus and vesicular compartment in the cytoplasm of choroid plexus cells (Miller *et al.*, 1999). In the brain endothelial cells, a large part of quinacrine was shown to be distributed and accumulated in the intracellular binding compartment (Fig. 2(B)). The resulting small part of quinacrine in the intracellular nonbinding compartment appears to contribute to the BBB permeability. The P-gp-mediated active efflux at the apical side of the plasma membrane and the large storage capacity in the cytoplasm are considered to restrict the entry of quinacrine into the brain. The mechanism involved in quinacrine transport at the basolateral side remains obscure.

In conclusion, quinacrine transport at the BBB is mediated by the influx and efflux transport systems. The influx of quinacrine is mediated by a pH-dependent and Na^+- and membrane potential-independent system, an OCTN1-like transporter. The efflux of quinacrine evoked by P-gp at the BBB restricts the entry of quinacrine into the brain. This phenomenon may be interpreted as lowering the therapeutic efficacy of quinacrine for CJD. This study may have clinical implications; quinacrine concentrations in the brain increased by P-gp modulators including verapamil may enhance the therapeutic efficacy of quinacrine for CJD.